Applied Environmental Research
- RESEARCH FOR SUSTAINABLE PLANET -

Research Article

Dual-Polarimetric Radar Applications for Investigating Severe Thunderstorms in Northern Thailand during the Pre-Monsoon Season

Nattapon Mahavik[1,*], Sarintip Tantanee[2], Fatah Masthawee[3]

[1] *Department of Natural Resources and Environment, Faculty of Agriculture Natural Resources and Environment, Naresuan University, Phitsanulok, Thailand*
[2] *Department of Civil Engineering, Faculty of Engineering, Naresuan University, Phitsanulok, Thailand*
[3] *Thai Meteorological Department, Bangkok, Thailand*

*Correspondence Email: nattaponm@nu.ac.th

Abstract

Understanding the physical characteristics of severe pre-monsoon thunderstorms is crucial for mitigating the adverse impacts of natural disasters on people in tropical regions. On April 23, 2020, a severe storm affected the Chiang Khong District of the Chiang Rai Province in Northern Thailand, causing devastation to more than 500 houses with hail and strong winds. This study investigated the storm's physical characteristics using dual-polarimetric radar data from the Thai Meteorological Department (TMD). Using a combination of polarimetric radar variables, such as reflectivity (Z_H), specific differential phase (K_{DP}), differential reflectivity (Z_{DR}), and copolar correlation coefficient (ρ_{hv}), fuzzy logic was utilized to classify the hydrometeor types. During the severe storm that affected the Chiang Khong District, hail and large raindrops were mixed in with the rain, according to the analysis. Two severe storms were observed in the unorganized mesoscale convective systems that were analyzed, with the second storm producing more intense effects due to the radar reflectivity shape of a bow echo that generated strong wind gusts. The Doppler radar data retrieved the wind field, indicating the convergence of intense local winds during the storm, which was consistent with the analysis results of synoptic-scale weather systems from ECMWF Reanalysis v5 (ERA5). In addition, a Hovmöller diagram revealed orographic enhancement of the convective cloud as the storm passed through mountainous regions prior to approaching the Chiang Khong District. The findings of this study can provide valuable information for TMD's near-real-time warning operation in order to minimize loss of life and property from future severe storms.

ARTICLE HISTORY
Received: 20 Sep. 2023
Accepted: 8 Dec. 2023
Published: 27 Dec. 2023

KEYWORDS
Polarimetric radar;
Pre-monsoon season;
Hail;
Wind gust;
Thailand

Introduction

Annually, severe thunderstorms give rise to meteorological disasters that impact individuals globally. These disasters encompass a range of destructive phenomena, such as intense precipitation, destructive wind gusts, tornadoes, hail, and lightning [1–6]. Hailstorms in the United States result in significant financial losses, reaching billions of dollars (USD) each year, impacting many sectors such as property, infrastructure, and agriculture [7–8]. According to a study conducted in Germany, the economic damages resulting from hailstorms surpassed a million dollars (USD). The research also revealed a consistent increase in the number of days with hail-related losses through-out Europe from 1990 to 2018 [9]. Severe thunderstorms occurring in India and Bangladesh during the pre-monsoon season (March-May) have been found to exhibit greater intensity compared to other seasons, leading to significant economic losses, property destruction, and loss of human lives [10–12].

Mesoscale convective systems (MCSs) are denoted as severe convective storms and are categorized as multi-cells,

which exhibit convergence in the lower troposphere and divergence at higher altitudes [13–14]. The convective multi-cell storm, which exhibits ordered characteristics, is commonly known as a squall line. This meteorological phenomenon has been extensively documented through the use of ground-based weather radar systems across several regions globally, including the Indochina Peninsula (ICP) situated in close proximity to Thailand [15–16]. Nevertheless, the ICP has not given sufficient attention to the strong convective multi-cell storm that is linked to hail occurrences in the pre-monsoon season. In order to examine this matter, Chantraket et al. [17] employed a S-band ground-based weather radar situated in Chiangmai, Northern Thailand. Their objective was to explore the correlation between hail occurrences and atmospheric instability inside pre-monsoon thunderstorms that transpired in 2012. Furthermore, Mahavik and Tantanee [18] conducted an analysis on the TRMM 16-year database utilizing radar satellite products in order to get insights into the physical characteristics of precipitation features (PFs) associated with MCSs in the ICP and its adjacent regions. It was discovered that the pre-monsoon season exhibited the greatest proportion of intense MCSs. According to various studies [10, 19–12], ground-based weather radar has demonstrated that the spatial extent of MCSs can vary from a few kilometers to several hundred kilometers, while their lifespan can range from less than an hour to multiple hours. Hence, the utilization of ground-based weather radar for comprehending the microphysical characteristics of intense thunderstorms in the pre-monsoon period inside the ICP region should facilitate the establishment of an effective warning system and the reduction of potential harm, casualties, and property damage.

The utilization of dual-polarization radar provides the benefit of acquiring data regarding the characteristics of hydrometeors, including their shapes, sizes, orientations, and phase status. This is achieved by employing two orthogonal polarizations to investigate clouds and precipitation [23–25]. Numerous research studies have been conducted to devise hydro-meteor classification algorithms (HCAs) utilizing fuzzy logic techniques. These algorithms aim to discern the types of hydrometeors by analyzing the backscattering data obtained from polarimetric radar variables. Notable contributions in this field include the works of [14, 19–20, 23, 26–28]. Although the Thai Meteorological Department (TMD) has established a comprehensive ground-based radar network that spans the whole nation, there has been less focus on comprehending the microphysics of precipitation during Thailand's pre-monsoon season, which falls in the midst of the Inter-Tropical Convergence Zone (ITCZ). In recent times, TMD has been progressively enhancing their terrestrial radar systems by transitioning from doppler weather radars to dual-polarization weather radars. The scarcity of literature on the utilization of dual-polarization weather radars for the analysis of severe thunderstorms in Thailand can be attributed to the recent advancements in radar systems. Nevertheless, the utilization of dual-polarization weather radars has the potential to enhance the efficacy of the real-time warning system in the pre-monsoon season.

Therefore, the objective of this research is to employ data obtained from dual-polarization weather radar in order to get a deeper understanding of the severe thunderstorm occurrences that transpired on April 23, 2020, within Chiang Rai Province, situated in the northern region of Thailand. The occurrence of a severe thunderstorm event led to the occurrence of strong wind gusts and hailstorms, which resulted in significant destruction to over 500 residential properties and agricultural areas in the Chiang Khong District. The paper is organized in the following manner: it begins with an introduction, followed by a section on the study area and data, then proceeds to detail the materials and methods employed. Subsequently, the analysis results are shown, followed by a discussion of these findings. Finally, the paper concludes by summarizing the study's key outcomes. The codes that we have generated for processing findings can be accessed at the following link:
https://github.com/nattaponm/hail_dualPol_Chiangkhong.

Study area and data

1) Study area

The geographical region under investigation in this study is situated in the northern mountainous regions of Thailand, as depicted in Figure 1. On the evening of April 23, 2020, the Chiang Khong District experienced a severe thunderstorm characterized by strong wind gusts and hailstorm. This meteorological event resulted in significant damage to more than 500 residential structures and agricultural fields. Data about the thunderstorm was collected using the Chiang Rai dual-polarimetric radar, which is controlled by the TMD. The region under investigation is renowned for its elevated likelihood of hail occurrences, as ascertained by the use of ERA-Interim reanalysis, as examined by Prein and Holland [6]. Nevertheless, the radar observation in the western region was impeded by the presence of mountain ranges, resulting in the initial scan of the Chiang Rai radar beam being obstructed by the topography. The geographical region under investigation undergoes three distinct climatic periods, specifically summer, rainy, and winter, with an intermediary phase between the summer and rainy seasons referred to as the pre-monsoon season. Okumura et al. [15] conducted an

investigation on the pre-monsoon season and found that numerous convective storms tend to occur in a dispersed manner, particularly in mountainous regions. These convective storms subsequently move eastward during the afternoon and nighttime. This eastward movement is attributed to the unbalanced surface heating and the influence of the prevailing wind, which blows from west to east.

Data

1) Digital elevation model (DEM)

A comprehensive examination was conducted on the obstruction of the beam caused by topographical features utilizing the Shuttle Radar Topography Mission Digital Elevation Model Version 4. Furthermore, a topographic analysis was performed utilizing a digital elevation model (DEM) to determine convective storm motion. The Shuttle Radar Topography Mission Digital Elevation Model (SRTM DEM) underwent pre-processing in the QGIS software. This involved the merging of individual tiles and the subsequent extraction of data within the defined study region using clipping.

2) Dual-Polarization radar

The Chiang Rai radar is located at geographical coordinates 19.961° N and 99.881° E, at an elevation of 389 meters above mean sea level (MSL). The utilization of the C-band frequency is observed in the operational context, whereby four successive scans are conducted at certain angles of 1.0°, 1.5°, 2.4°, and 3.4°, as depicted in Table 1. The instrument has the capability to monitor meteorological conditions within a range of 240 km, with a temporal resolution of four scans per hour. The study utilized a total of 96 radar files in the universal format (UF). There are a total of eight radar variables, namely "reflectivity," "velocity," "spectrum width," "corrected reflectivity," "corrected differential reflectivity," "differential phase," "cross-correlation ratio," and "specific differrential phase." In this section, we present a concise explanation of dual-polarization variables in order to comprehend the microphysical attributes of MCSs. Differential reflectivity (Z_{DR}) offers insights into the typical morphology inferred from reflectivity measurements, enabling estimation of the median diameter of raindrops. The specific differential phase (K_{DP}) parameter offers insights into the concentration of liquid water. The copolar correlation coefficient (ρ_{hv}) is utilized to quantify the similarity or mixture of observed items within each volume by comparing the pulse characteristics in both horizontal and vertical planes [29–30].

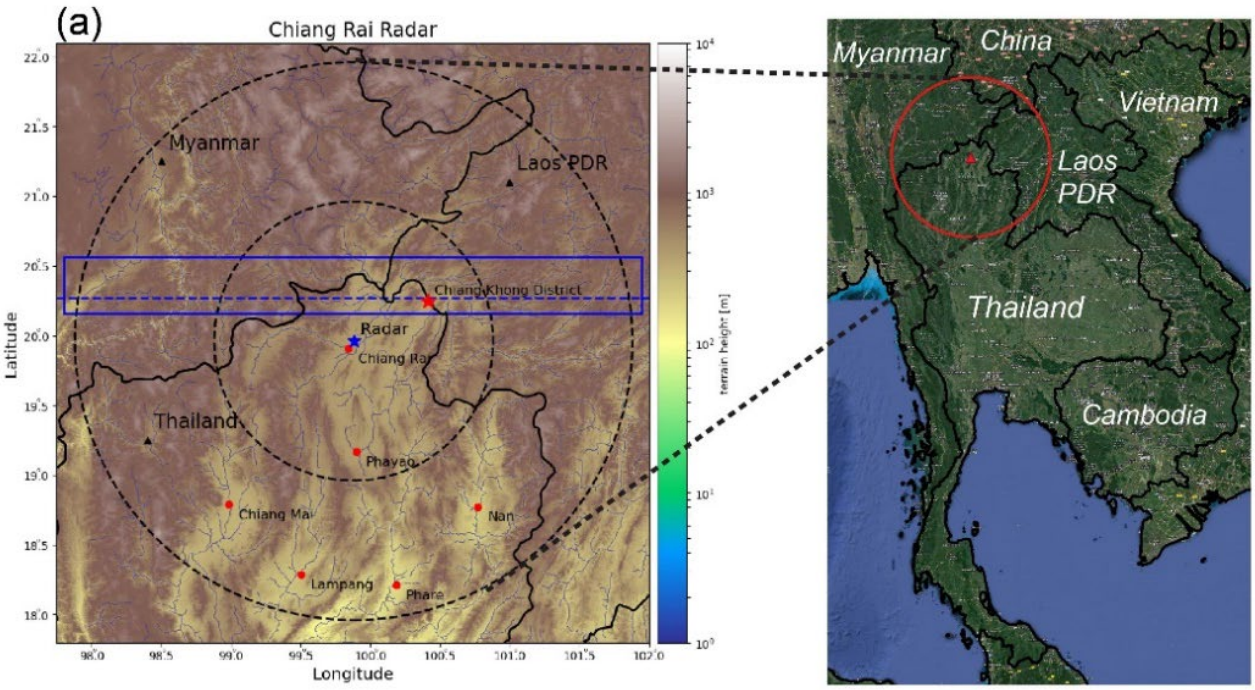

Figure 1 Study area in northern Thailand's Chiang Rai Province (a) the Chiang Rai radar location is marked by a blue star. Dashed circles indicate the 120 km and 240 km observation radii of the Chiang Rai radar. The red star shows the location of Chiang Khong district. A blue dashed line marks the longitudinal slicing line used to create the vertical profiles shown in Figures 6 and 7 (details in text). The blue box indicates the area where data was used to create the Hovmцller diagram in Figure 9 (details in text) (b) map overview of the study area.

3) ECMWF reanalysis data

No upper air soundings were observed in the study area during the storm event. Temperature profiles were produced utilizing the European Centre for Medium-Range Weather Forecasts (ECMWF) reanalysis data ERA5, as described by Hersbach [31]. ERA5, the fifth iteration of the atmospheric reanalysis developed by the European Centre for Medium-Range Weather Forecasts (ECMWF), supersedes the preceding ERA-Interim reanalysis. It is currently accessible via the Copernicus Climate Change Service, as of 2017 [32]. The ERA5 dataset has been extensively employed in the examination of intense weather events, as demonstrated by the studies conducted by the Copernicus Climate Change Service [32] and Romanick et al. [33]. The thermodynamic study and classification of hydro-meteor types involved the utilization of five atmospheric variables. These variables, namely geopotential, U wind, V wind, temperature, and relative humidity, were picked at all pressure levels in close proximity to the Chiang Khong district. Materials and Methods

Software

The spatiotemporal resolution of data obtained from ground-based weather radar is very high in terms of scanning frequency and spatial resolution. For data analysis, it is necessary to have a well-managed processing. Python was chosen for analysis because it can manage vast data arrays and support a variety of tasks with open-source radar libraries. For scientific researchers are now available Python radar library packages. Our analysis employs the open-source radar libraries Py-Art [35-36]. QGIS was utilized for DEM preprocessing.

Method

The main work flow of the study is shown in Figure 2. There are four main steps in the present study for the severe storm analysis as followings:

1. Pre-processing radar data
2. Pre-processing reanalysis data to create temperature profile
3. Hydrometeor identification
4. Physical analysis of hail storm

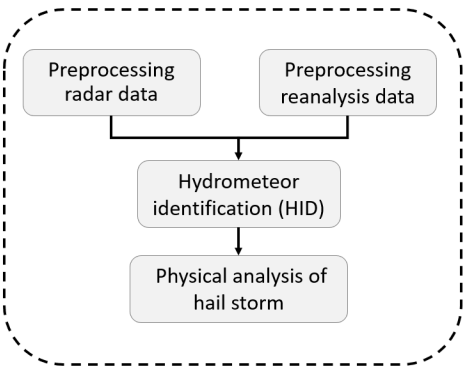

Figure 2 Main workflow of the study.

1) Pre-processing radar data

Radar data preprocessing is a crucial step prior to analysis. On the day of the storm, a total of 96 radar data files were acquired, and the pre-processing phase was carried out using open-source radar libraries, namely Wradlib and Py-Art, with the following steps:

- SNR for clutter/noise removal for reflectivity
- KDP (specific_differential_phase) is retrieved from differential_phase
- KDP is corrected using the "phase_proc_lp" method developed by applying Linear Programming to Polarimetric Radar Differential Phase Processing, as described by Giangrande et al. [37].
- attenuation for reflectivity is corrected

Before using the polarimetric radar variables for further physical analysis of the severe storm, they must be corrected. For the processing duties, the Py-Art radar library was used.

2) Signal to noise (SNR) to remove clutter/noise for reflectivity

The raw reflectivity data often contains extraneous signals and interference that are not related to meteorological phenomena. The application of the signal to noise tatio (SNR) approach was utilized to eliminate clutter and noise from the reflectivity data. In order to achieve favorable outcomes in the elimination of clutter and noise, the analysis focused on the top of atmosphere (TOA) at an altitude of 15,000 meters above the Earth's surface, as observed from the radar station.

3) Computation of specific differential phase (K_{DP})

The retrieval of K_{DP} was performed by utilizing the Py-Art library, which is based on the methodology proposed by Maesaka et al. [38], to process the Φ_{DP} data. The K_{DP} parameter holds significant importance in polarimetric radar analysis for the purpose of classifying hydro-meteor kinds through the utilization of the Fuzzy logic methodology. The K_{DP} algorithm was refined using Linear Programming in the Py-Art software package, following the methodology outlined by Giangrande et al. [37]. This approach also enables the retrieval of Φ_{DP}.

4) Attenuation correction of reflectivity

The reflectivity was further adjusted using the Py-Art software, employing the Z-PHI technique as described by Gu et al. [39]. This method also yielded the copolar correlation coefficient (ρ_{hv}) and the corrected Φ_{DP}.

5) Classification hydrometeor types

In order to get insight into the microphysics occurring during a severe storm, the researchers employed

pre-processed polarimetric radar variables and temperature profiles to categorize different forms of hydrometeors. The classification was performed using the hydrometeor identification (HID) technique based on fuzzy logic, which has been utilized in earlier research [19–20, 40]. The HID method was constructed by researchers affiliated with the Radar Meteorology Group at Colorado State University, commonly referred to as CSU Radar Tools.

6) Construct temperature vertical profile

Due to the unavailability of atmospheric sounding data in proximity to the designated study region, the researchers obtained ERA5 reanalysis data corresponding to the storm event at 1800 Local Standard Time (LST) in order to establish the vertical temperature profile. A Python script was created to compute the parameters using the acquired data and generate the appropriate format adhering to the Wyoming standard for visualizing the SkewT/logP graph in the MetPy module, as depicted in Figure 3.

7) Fuzzy logic method

The utilization of the fuzzy-logic approach has been demonstrated in the classification of hydrometeor types inside a radar volume scan, as evidenced by the studies conducted by several groups [41–43]. The utilization of radar variables, specifically Z_H, Z_{DR}, K_{DP}, and ρ_{hv}, is employed in the construction of membership functions (MFBs) corresponding to the various hydrometeor types linked to the temperature profile. The hydrometeor type with the highest fuzzy score will be selected as the representative for the given grid. The calculation of the fuzzy score for each hydrometeor type involved the utilization of the fuzzy-logic equation, which was derived from the MBFs proposed by Dolan and Rutledge in 2009.

$$\beta = \frac{1}{1+\left[\left(\frac{x-m}{a}\right)^2\right]^b} \quad \text{(Eq. 1)}$$

Where, a is the denotes width, m is the middle value, b is the slope, and x is the observation data.

The polarimetric radar variables (K_{DP}, Z_{DR}, ρ_{hv}) were weighted (W) with values of 1.0, 0.8, and 0.1. The overall score for each hydrometeor type (μi) was calculated by multiplying the derived weighing scores by the ZH and T scores, as shown in the equation:

$$\mu_i = \left[\frac{(W_{Z_{dr}}\beta_{Z_{dr},i}+W_{K_{dp}}\beta_{k_{dp},i}+W_{\rho_{hv}}\beta_{\rho_{hv},i})}{W_{Z_{dr}}+W_{K_{dp}}+W_{\rho_{hv}}}\right]\beta_{T,i}\beta_{Z_h,i} \quad \text{(Eq. 2)}$$

Where, i is the represents hydrometeor types, W is the represents the weight of each polarimetric radar variable, and β is the represents the score based on DR09's equation for each variable set and each hydrometeor type.

8) Beam blockage analysis

In order to comprehend the impact of topography on the observation radar beam, a simulation was conducted to analyze the propagation of the radar beam as it interacted with the SRTM DEM Version 4. This simulation was based on the utilization of the following equation.

$$H = \sqrt{r^2 + R'^2 + 2rR'sin\emptyset} - R' + H_0 \quad \text{(Eq. 3)}$$

In radar observation, H is the observation height, r is the distance from the measured point, ш is the beam elevation angle, H_0 is the tower height, R is Earth's radius, and R' is 4/3 of R. First elevation beam responses to topography (Figure not shown). In the northwest of the radar site, topography hindered the radar beam by over 90%. This study focused on Chiang Khong District, although the topography east of the radar station did not hinder radar beam observation.

Analysis results

1) synoptic-scale weather analysis and atmospheric instability

Analysis of synoptic-scale weather systems three days before the severe storm and on storm day can show the dynamic processes that caused it. The synoptic maps utilizing ERA5 reanalysis data at 0700 LST showed a warm airmass throughout Indochina's inland, including the research area. A northeasterly cold air mass was traveling from central China to Indochina (Figure not shown). Cold air with high density collided with neighboring warm air that had lesser density. In the pre-monsoon season, air mass density differences may trigger severe storms.

Anticyclonic wind was observed between Laos PDR and Cambodia on April 20-22, 2020. The north of Thailand was receiving moist air from Indochina. The middle of China airmass was weak and did not affect Indochina. Southerly wind from the Gulf of Thailand and westerly wind from the Gulf of Bengal in northern Thailand converged at 850 hPa, creating an enormous anticyclonic wind in the Gulf. This matches the 1998 pre-monsoon study reported by Kiguchi and Matsumoto [44]. China's cold air mass intensified from April 20 to 23, 2020. The cold air mass wedge penetrated into Indochina, causing local warm air mass to convect over mountain ranges and flat plains.

Table 1 reveals the computed atmospheric instability indices for April 20-23, 2020, near the time of the storm occurrence at 1800 LST, based on ERA5 reanalysis data. Evidently, the calculated values of all indices on April 23, 2020, exceeded the critical threshold. The storm day's indices indicated favorable atmospheric conditions for the occurrence of severe storms.

Compared to the previous three days, the CAPE value for April 23, 2020 was relatively high and classified as extremely unstable. CAPE indicates the high quantity of buoyant energy available to accelerate a parcel vertically, as shown in Figure 3. In addition, as shown in Figure 3(d), there was a strong wind shear from low-level winds to the midsection of the atmosphere.

Dual polarimetric radar and doppler on the severe storm

1) Physical characteristics of the severe storm

During the 18:45 LST radar scan, two convective storms were observed impacting the study area, specifically the Chiang Khong districts. In Figure 4, the first storm had passed east of the study area, while the second storm was approaching Chiang Khong. As shown in Figure 4(a), the intensity of reflectivity based on Z_H for the storms exceeded 50 dBZ. For the second the storm, the bow echo reflectivity was observed. Consequently, the wind gust was observed in the direction of the storm's forward motion, impacting the properties of local residents. Such a bow echo could produce a powerful downburst or tornado [1, 45–46]. In addition, when the moist air encountered the frigid pool created by evaporative cooling of the downdraft, the updraft could experience a significant influx of air. In such a case, convection may result from the forcible ascent of inflow air into the updraft [47].

As depicted in Figure 4d, the first elevation's KDP values exhibited a high positive range of 2-4 deg km^{-1} in the second storm's observed area. This result was comparable to the K_{DP} of the first storm, which also had a positive value that was quite high. Due to its ability to detect equal phase shifts on polarized horizontal and vertical waves, K_{DP} is used to detect heavy rainfall contaminated with hail because it can detect small hail mixed with rain [24–48]. According to the classification of precipitation according to the four elevations, hail and large raindrops were obviously mixed. As shown in Figure 4(f), large hail areas were observed in the fourth elevation angle. The second storm produced a larger hail area than the first. At lower elevation angles, melting hail was observed with diminishing hail areas replaced by rain and large droplets. However, the first elevation still observed a mixture of hail and droplets that were large in size.

Table 1 Atmospheric instability indices

Instability indices	Critical level	20 April 2020	21 April 2020	22 April 2020	23 April 2020
CAPE (J kg^{-1})	> 1,000	244.19	36.95	190.35	4,544.19
Lifted-Index (°C)	< -3	-1.56	-0.05	-0.89	-9.35
K-Index (°C)	> 30	34.13	29.63	32.84	36.46
TT-Index (°C)	> 45	47.12	45.83	46.24	49.74

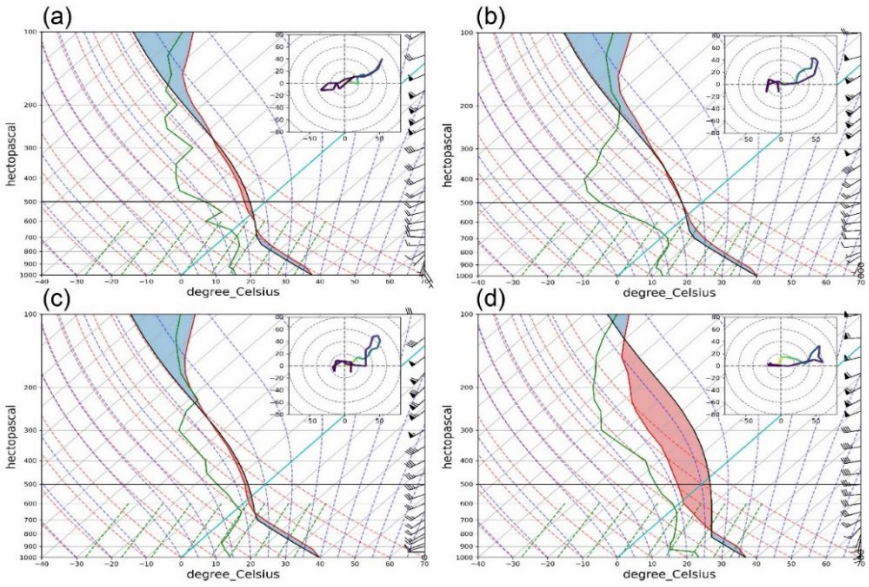

Figure 3 Thermodynamic diagram (Skew-T log-P diagram) for 20-23 April 2020 at 1800 LST, close to the time of the storm occurrence on 23 April 2020. All variables used in the diagram are from ERA-5 reanalysis data extracted near the geographic coordinates of Chiang Khong District. The red-shaded areas indicate the CAPE values. Wind data for all atmospheric levels is indicated by wind barbs.

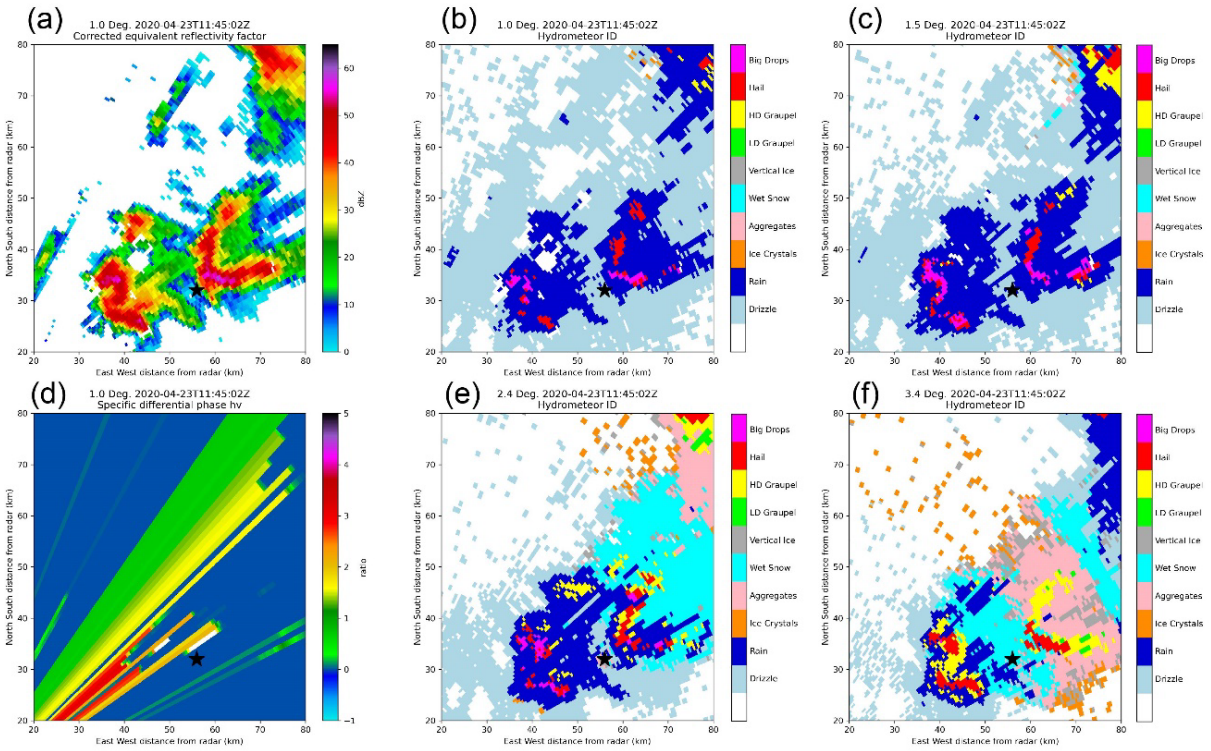

Figure 4 Example of classified hydrometeor types for all four elevation angles using Fuzzy logic method at 1845 LST on 23 April 2020. (a) radar reflectivity for the first elevation angle, (b) classified hydrometeor types for the first elevation angle (c) classified hydrometeor types for the second elevation angle, (d) specific difference phase for the first elevation angle, (e) classified hydrometeor types for the third elevation angle, and (f) classified hydrometeor types for the fourth elevation angle. Black star indicates location of Chiang Khong District.

2) Storm evolution of classified hydrometeor types

The severe convective storm was detected for the first time in mountain ranges west of the radar station. Three groups of storms were observed to the west of the radar station at approximately 1700 LST, as depicted in Figure 5 at the first elevation radar angle of 1.0°. These disorganized storms moved towards the Chiang Khong District from the east. On the Hovmцller diagram, it was observed around 1500 LST that storm clouds were present, but they did not appear to be moving until 1700 LST (Figure 9). The radar then detected these convective storms moving toward the east. Based on the results of classified hydrometeors, hail was observed within the storm clouds at 1700 LST, while the storm area grew to approximately 40 x 40 km by 1745 LST as it moved eastward from the radar.

In accordance with the cloud morphology classification scheme [49], isolated cells (IC) were observed between 1700 and 1800 LST, followed by a cluster of cells (CC). The storm clouds appeared to organize by merging clouds around 1800 LST, following an isolated cloud in the southwest of the large cloud at a distance of around 20 km. Before 1800 LST, the complex multicell system had a leading stratiform (LS) with convective clouds behind the system, but at 1800 LST, the convective regions organized themselves to the system's right, perpendicular to the Chiang Khong District. At approximately 18:15 LST, the first storm moved towards the Chiang Khong District, bringing with it hydrometeors classified as hail mixed with large droplets and rain. The second storm did not reach until 1915 LST, bringing with it larger hail areas and strong wind gusts. At 18:45 LST, prior to the onset of the second storm, a bow echo was detected in the radar reflectivity.

At 1815 LST, the first damaging storm appeared southwest of the large cluster of thunderstorms. It was classified as a mixture of massive raindrops and hail. As the second damaging storm, a larger area of the storm cloud accompanied by more hail was observed at 1915 LST. As evidenced by a bow echo in the radar reflectivity at 1845 LST, it was reported that strong winds occurred prior to the approaching storms.

In general, the classified hydrometeor types indicate that the storm cloud type is LS, with the convective cloud located ahead of the stratiform cloud. In such storms, the strong front-to-rear wind can be observed from the ground to the center of the storm [50]. Notably, the first damaging storm exhibited a cloud morphology resembling Training Line-Adjoining Stratiform (TL/AS) [13] with an organized convective cloud adjacent to the system.

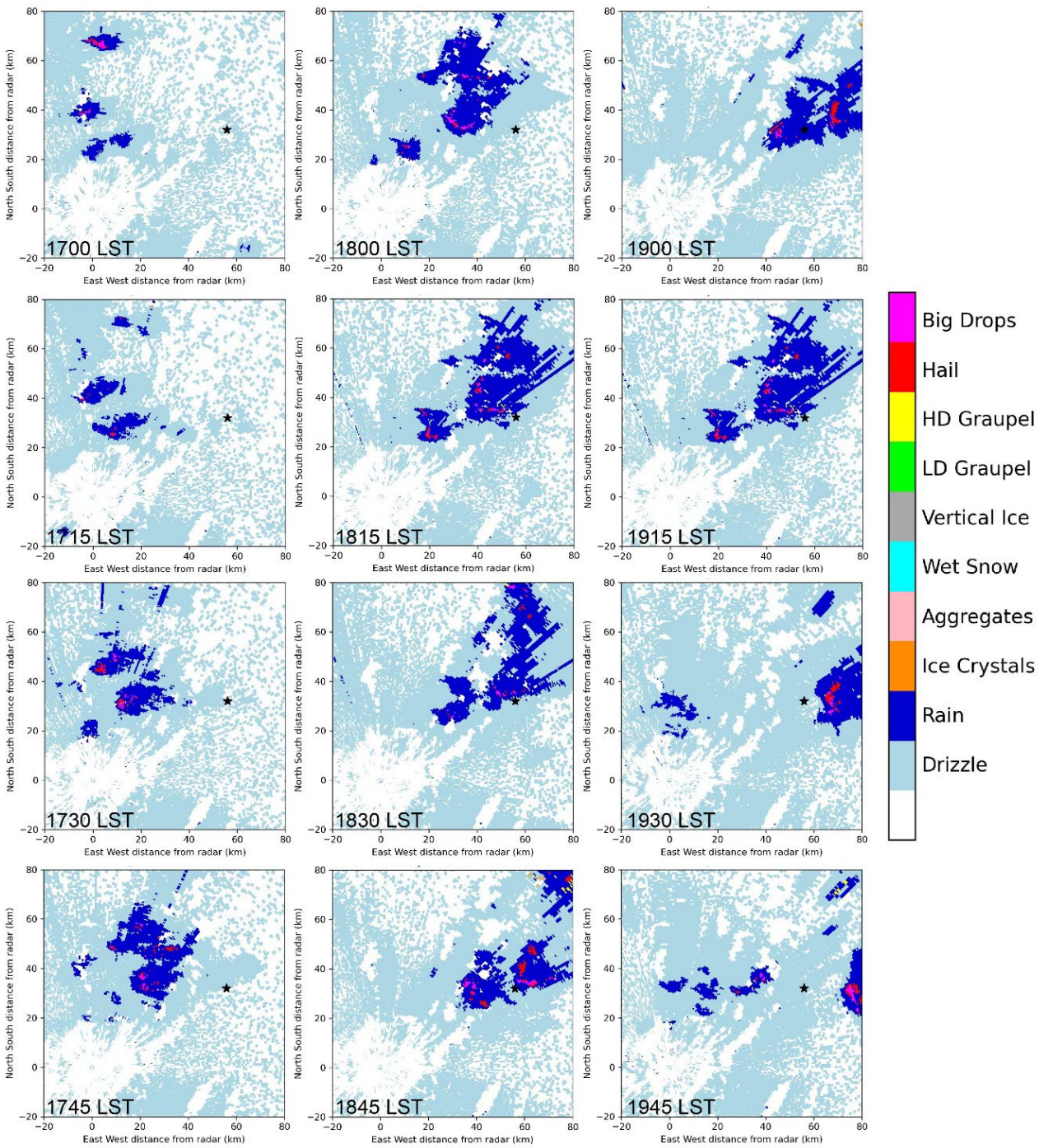

Figure 5 Evolution of storm hydrometeor classification using the first elevation angle from 1700 LST to 1945 LST on 23 April 2020. The location of Chiang Khong District is indicated by a black star.

3) Analysis of vertical storm structure

Despite the fact that the Chiang Rai radar has only four elevation angles, analyzing the vertical storm structure can help reveal the storm's physical characteristics. The radar data was constructed at each 250-meter height level, for a total of 44 levels from the earth to an altitude of 11 km. As shown in Figures 6 and 7, vertical profiles of the storm were synthesized using all levels of the constructed gridded data in the Chiang Khong District for 1830 LST and 1915 LST, respectively. To generate the profiles, dual-polarimetric parameters such as Z_H, ρ_{hv}, and Z_{DR} were chosen.

Using reflectivity data from four elevations does not provide a comprehensive comprehension of the damaging storm's cloud top height. As shown in Figure 6(a) of the 1830 LST, the vertical profiles demonstrate reflectivity exceeding 50 dBZ above 3 km. The observed incline of the storm core to the front of the storm motion clearly demonstrates a correlation with the outflow wind of the storm top and the horizontal wind on the ground at the same time [51]. In Figure 6b, the ρ_{hv} values ranged from 0.70 to 0.95 at a distance of 50 km from the radar, indicating the presence of hail, which is consistent with Anderson et al. [3], who observed hail signatures using

C-band dual-polarimetric radar. At a distance of 50 to 60 km, the Z_{DR} showed values in the range of 2-4 dB, indicating the merging of large raindrops and hail.

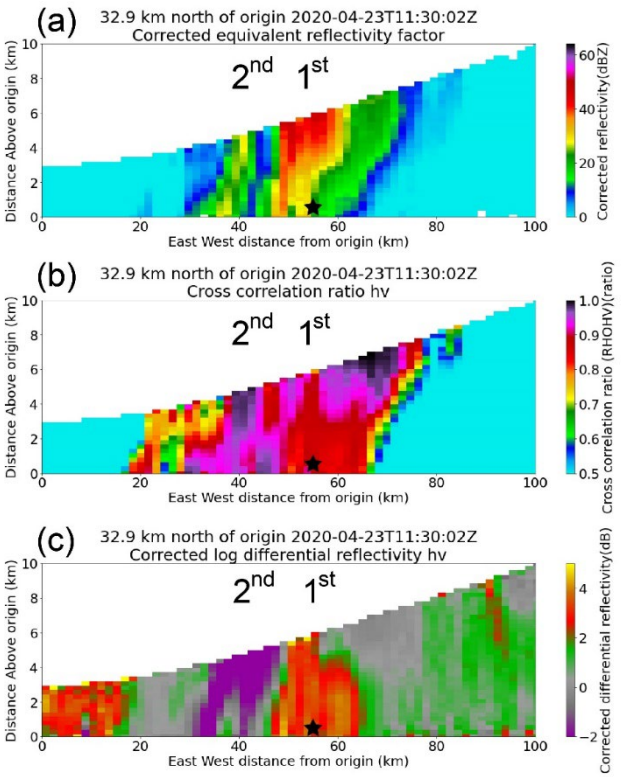

Figure 6 Vertical profile obtained from four elevation sweeps of Chiang Rai radar along the longitudinal line as indicated in Figure 1 at 1830 LST on 23 April 2020. (a) Corrected radar reflectivity. (b) Copolar correlation coefficient (ρ_{hv}). (c) Differential reflectivity (Z_{DR}). The black star indicates the location of Chiang Khong District.

The presence of hail in the second destructive storm at 1915 LST is evident from the vertical profiles of the three parameters, as depicted in Figure 6. The radar reflectivity Z_H in the vicinity of Chiang Khong and its adjacent areas has surpassed 50 dBZ, exhibiting more intensity compared to past instances, following the passage of the initial storm. The ρ_{hv} values in close proximity to the convective storm core exhibited a range of 0.7 to 0.95, whilst the ZDR values were around 4 dB. Both values signify the presence of hail, which was also examined by Anderson et al. [3].

Typically, Z_{DR} columns, characterized by vertical columns exhibiting significant Z_{DR} values above the freezing 0°C limit, have been identified as potential indicators of the existence of sizable supercooled raindrops, as well as water-coated hail or ice [30, 52–55]. The combined utilization of Z_{DR} and K_{DP} has been employed for the purpose of detecting the existence of hail and making an estimation of its dimensions [56–57]. In the instances under consideration, as documented at 1915 LST in Figure 7(c), it was noted that the Z_{DR} values in close proximity to the Chiang Khong area exhibited a considerable elevation. Furthermore, the Z_{DR} column surpassed a distance of 5 km, beyond the freezing level as depicted in Figure 3. The Z_{DR} column provides unequivocal evidence of the existence of hail within the storm cloud.

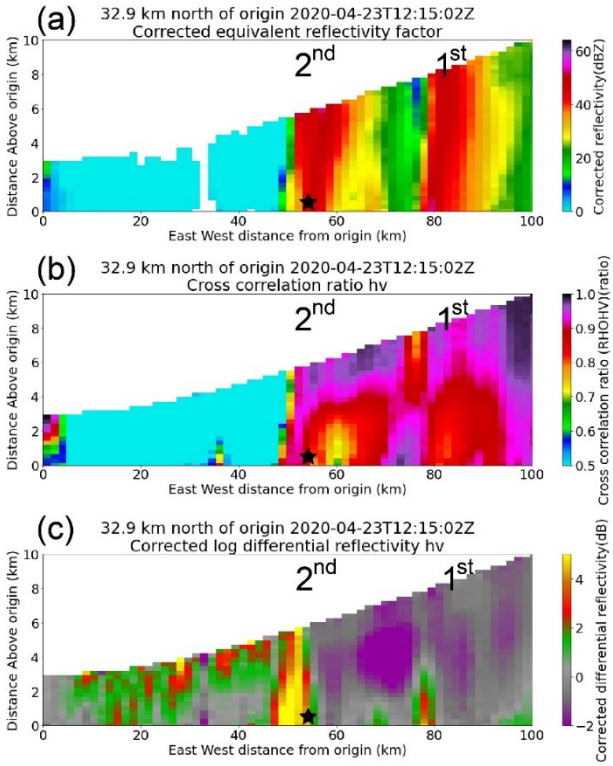

Figure 7 Vertical profile using four elevation sweeps of the Chiang Rai radar along the longitudinal line as indicated in Figure 1 at 1915 LST on 23 April 2020. (a) Corrected radar reflectivity. (b) Copolar correlation coefficient (ρhv). (c) Differential reflectivity (ZDR). The black star indicates the location of Chiang Khong District.

4) Topographic analysis on the storm

Using a Hovmцller diagram, the storm's velocity and intensity for mean and maximal reflectivity were analyzed. As depicted in Figure 1, the diagram was produced using a Constant Altitude Plan Position Indicator (CAPPI) at 2 km during 1400-2300 LST by averaging the distance along the x and y axes.

Based on the average reflectivity of the Hovmцller diagram (Figure 8(a)), the storm's velocity was approximately 11 m s^{-1} or 40 km h^{-1}. The storm was moving beyond the Chiang Rai radar's observed radius of 240 km and into Laos PDR. This storm velocity is consistent with that witnessed in squall lines west of the Indo-China Peninsula [15, 58–59] found some similarities between the observed squall lines in the west of the Indo-China Peninsula and those in the United States that originated on the leeward side of mountainous regions.

However, storm systems in Indo-China were smaller than 100 km^2 and lasted less than a day, while those in the United States were larger than 1,000 km^2 and persisted longer than a day. [15] hypothesized that these moving storms may contribute to the daily variation of rainfall in inland Indo-China during the summer. Nevertheless, if we only consider the speed of the hail-producing thunderstorm in our case with the storm case in Croatia as a mid-latitude region, we may discover a speed of 28 km h^{-1} [60].

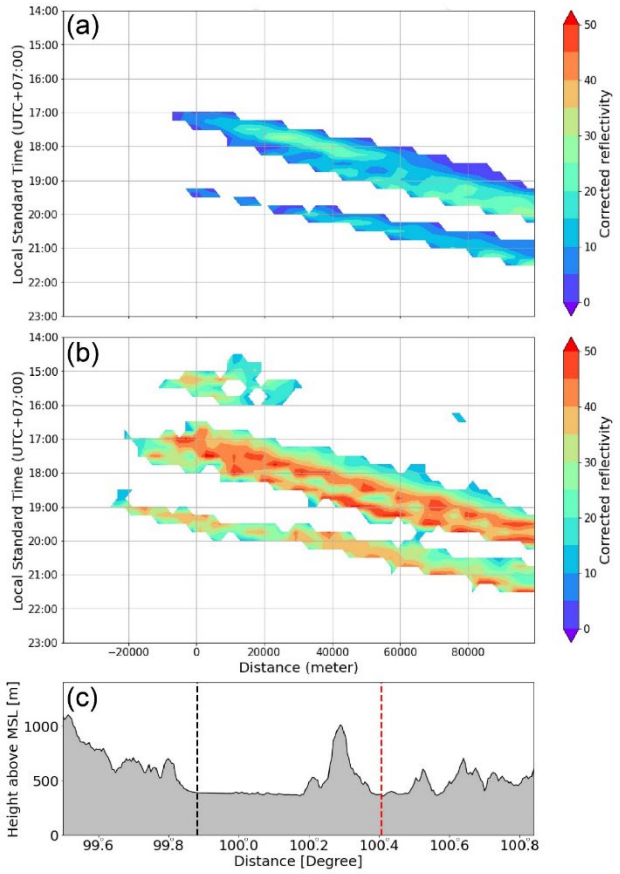

Figure 8 Hovmцller diagram for storm intensity analysis and topographically induced severe wind gusts using radar areas indicated in Figure 1. (a) Mean reflectivity. (b) Maximum reflectivity. (c) Topography retrieved from SRTM DEM along the line indicated in Figure 1. The dashed black and red lines indicate the locations of the Chiang Rai radar site and Chiang Khong District, respectively.

Figure 8(a) depicts two moving cyclones, both originating from the western mountain ranges. At around 1700 LST, the first storm system moved east of the radar observation. The second storm system occurred in the same area as the first storm at 1900 LST, but there were no reports of damage. The maximum reflectivity (Figure 8(b)) differed from the mean reflectivity (Figure 8(a)) when three storm systems were observed at various periods. At 15:00 LST, virtually stationary afternoon storms were observed, moving only briefly. As depicted in Figure 8b, the storm that began at 1700 LST had two sub-storms that approached the Chiang Khong District at separate times. As depicted in Figure 5, the storm systems were initially concentrated around 1,700-1,800 LST but separated into two systems at a distance of 20 km from the radar site.

As depicted in Figure 8(b), the second storm's intensity increased from 1845-1915 LST as it approached mountainous regions from a distance of 40 to 60 km. Figure 9 depicts that severe wind surges were also observed at 1915 LST due to the bow echo of radar reflectivity. Chiang Khong district, located on the leeward side, was damaged by the approaching wind gusts and hail storms as a result of orographic enhancement of the thunderstorm systems.

Due to the prevalence of very tall convective clouds in mountainous regions, there is a relationship between topography and hailstorm occurrence. Rasmussen et al. investigated severe convection and lightning in subtropical South America using TRMM-PR and discovered that communities in the Andes Mountains, such as Mendoza and Cyrdoba, are frequently subject to hailstorms [4]. These severe hailstorms have caused significant damage to agricultural products, prompting the Argentine government to initiate a project to support agriculture insurance and prevent hailstorms through cloud-seeding efforts by aircraft.

Furthermore, hailstorms are common in complex mountainous regions, comparable to our study area. As depicted in Figure 9, the convergence of low-level wind was also evident when using doppler-retrieved wind field, which is consistent with previous studies in the southwest of Germany. Pocakal et al. [61] discovered that hailstorms were caused by the convergence of winds over mountainous regions. Kunz and Kugel discovered that hailstorms in the Black Forest were consistent with high spatial variability based on ground-based weather radar measurements [2].

Discussion

In addition to producing hail, the severe storm also produced damaging gusts that damaged homes in the Chiang Khong district. Using Doppler velocity data, an analysis of atmospheric turbulence at low levels was conducted. PyTDA implemented an algorithm from the NCAR Turbulence Detection Algorithm (NTDA) to compute Eddy Dissipation Rate (EDR) [62–63]. The NTDA performs data quality control using radar reflectivity, radial velocity, and spectrum width in conjunction with fuzzy logic to correct and normalize the data. Using long- and short-range equations, EDR can then be derived [64].

Doppler data are utilized to calculate wind vectors in the analysis of low-level winds using the Python-based Single Doppler Retrieval Toolkit (SingleDop) [65]. The cross-covariance function between the radar radial and tangential components (relative to the direction of the radar beam) of background wind errors is derived in two dimensions. As initial data, the dealiased velocity doppler data from the first elevation angles was used to determine the wind vector.

The results of EDR during the storm that brought two convective storms to the Chiang Khong District have been estimated based on 1830 to 1915 LST, as depicted in Figures 9(a-d). Due to the convective clouds produced by the convective storms, EDR values have correlated with high reflectivity. As depicted in Figure 9(e-h), the synthesized wind vector from velocity doppler has been computed. At 1830 LST, it was discovered that powerful westerly winds and southerly winds were converging on convective clouds. At 1915 LST, the wind velocity has increased, exceeding 10 m s^{-1}. These winds originated from the northeast, which corresponded to the storm's trajectory in the Chiang Khong District.

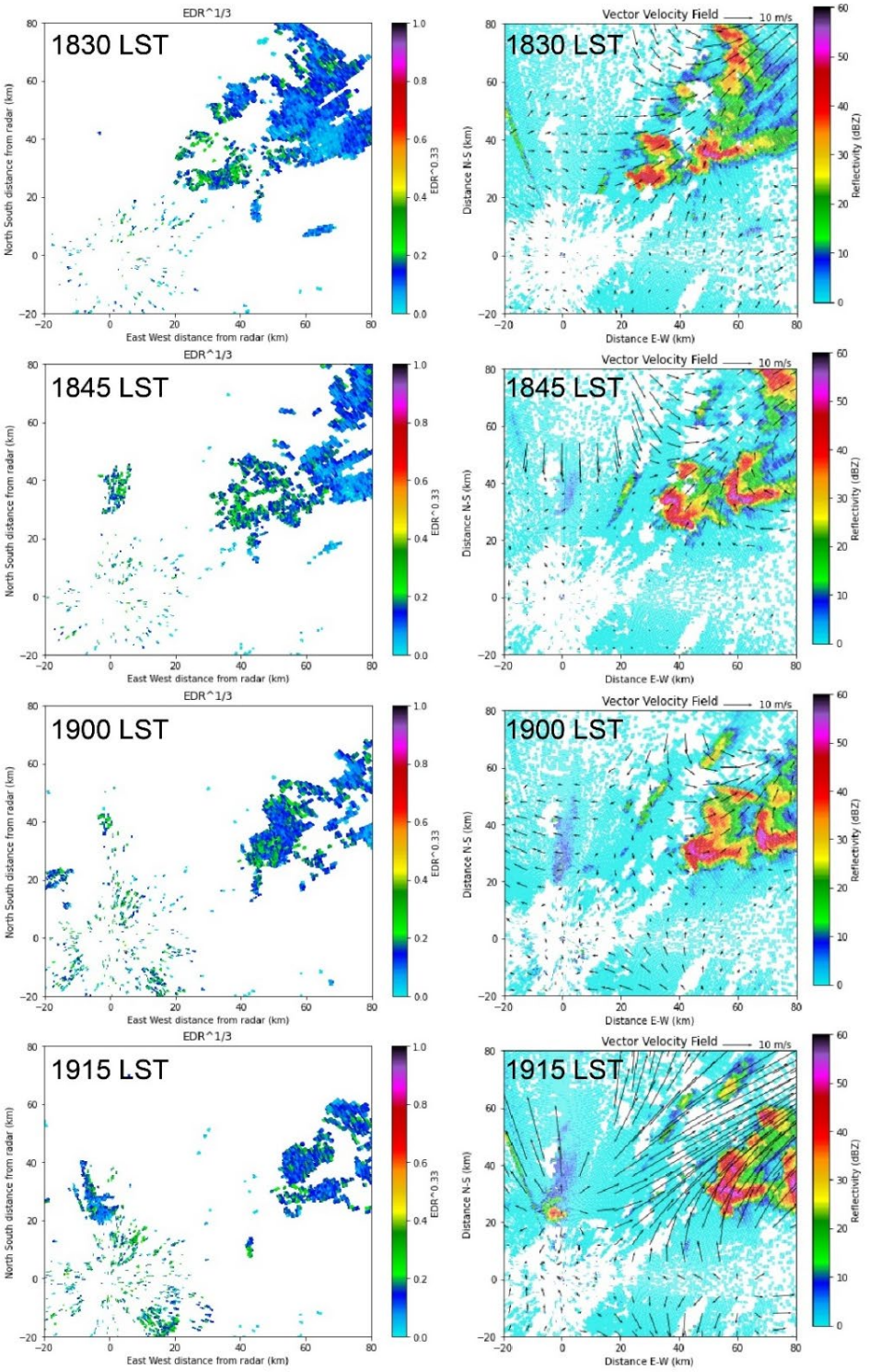

Figure 9 Wind analysis during storm occurrence affecting Chiang Khong district. (a-d) Wind turbulence from 1830-1915 LST. (e-h) Wind vector field retrieved from Doppler velocity from 1830-1915 LST.

At 1915 LST, a bow echo of radar reflectivity was observed with a length of around 30 km. The strong low-level wind was found to be greater in front of the second storm due to downdraft than the observed wind of the first storm, causing damage to more than 500 families' houses. Bow-shaped convective systems cause strong downdraft wind at the bow echo apex due to rear-inflow wind, according to Wheatley et al. [66]. Low-level mesovortices within the bow echo could generate damaging surface winds in a direct line. In addition to revealing strong winds, the bow echo can also generate downbursts that may be caused by squall line type or single-cell type [1, 67]. Microbursts and macrobursts are the two classifications of downbursts. In previous studies, there was evidence that microburst-produced surface winds in a straight line caused damage to agricultural areas [1, 45, 67]. In our case, a downburst may have contributed to the devastation in the Chiang Khong district. No fieldwork was conducted after the damaging event, and the damage assessment did not specify the actual cause of the damaging wind.

According to Mathias et al. [68], there is a potential for a decrease in casualties and property damage through the utilization of high-resolution regional model hindcasts in the western region of Germany. This would involve the forecasting of thunderstorms that exhibit a bow echo shape. The utilization of dual-polarimetric radar observations would additionally serve the purpose of promptly issuing warnings, while the preservation of radar data can facilitate the analysis of tropical extreme occurrences, hence providing insights into the physical attributes of severe storms.

Conclusions

This study provided a comprehensive analysis of a severe storm that impacted the Chiang Khong District in northern Thailand in April 2020, during the pre-monsoon season. Utilizing dual polarimetric radar observations, ERA5 reanalysis data, and synoptic-scale meteorological analysis, this study elucidated key factors contributing to the storm's intensity. The study identified hail, wind storms atmospheric instability, and convective orographic enhancement as crucial elements in the formation and development of the storm. The key finding of our study is that the application of the Fuzzy logic method to classify hydrometeor kinds at all four elevation angles indicated the presence of hail, which is associated with the emergence of a bow echo shape. In addition, it demonstrated the practical utility of open-source Python libraries for operational forecasting and warning systems, highlighting the significance of expanding radar capabilities for more precise storm tracking and the need for upper air sounding data to improve the classification of hydrometeor types. Beneficial to the Thai people, this research sets the groundwork for improved disaster preparedness and mitigation strategies in mountainous regions prone to severe storms.

In conclusion, the findings of this research provide important insights into the comprehension and forecasting of severe storms, particularly in regions with complex topography, such as northern Thailand. We can better protect communities and infrastructure from the effects of severe pre-monsoon storms by enhancing our understanding of these weather phenomena and the instruments available for analysis and prediction. This research not only contributes to the scientific comprehension of such events but also has practical implications for improving early warning systems and disaster management protocols, ultimately increasing the resilience of the affected areas.

Acknowledgements

We would like to extend our heartfelt gratitude to the anonymous reviewers for their invaluable remarks and productive discussions, which greatly enhanced the overall quality of this research. We deeply appreciate the Office of the Permanent Secretary, Ministry of Higher Education, Science, Research, and Innovation for providing full financial support under Grant No. RGNS63-136 for this research work. We would like to express our appreciation to the Thai Meteorological Department for their contribution of radar data, which was utilized in the course of this research. We express our gratitude for the support received in utilizing the PyTDA library, which was generously given by Dr. Timothy Lang from NASA's Marshall Space Flight Center. The figures in this study were mostly produced using the utilization of Python scripts, together with the Metpy library, as well as two open radar libraries, namely Wradlib and Py-Art.

References

[1] Fujita, T.T. Manual of downburst identification for project NIMROD. University of Chicago SMRP Research Paper, 1978, 156, 104 pp.

[2] Kunz, M., Kugel, P. Detection of hail signatures from 3D C-Band radar reflectivity. Atmospheric Research, 2015, 153, 565–577.

[3] Anderson, M.E., Carey, L.D., Petersen, W.A., Knupp, K.R. C-band dual-polarimetric radar signatures of hail. Electronic Journal of Operational Meteorology, 2011, 12, 1–30.

[4] Rasmussen, K.L., Zuluaga, M.D., Houze, R.A. Severe convection and lightning in subtropical South America. Geophysical Research Letters, 2014, 41, 7359–7366.

[5] Cecil, D.J., Blankenship, C.B. Toward a global climatology of severe hailstorms as estimated by satellite passive microwave imagers. Journal of Climate, 2012, 25, 687–703.

[6] Prein, A.F., Holland, G.J. Global estimates of damaging hail hazard. Weather and Climate Extremes, 2018, 22, 10–23.

[7] Changnon, S.A., Burroughs, J. The tristate hailstorm: The most costly on record. Monthly Weather Review, 2003, 131, 1734–1739.

[8] Brown, T.M., Pogorzelski, W.H., Giammanco, I.M. Evaluating hail damage using property insurance claims data. Weather, Climate, and Society, 2015, 7, 197–210.

[9] Pucik, T., Castellano, C., Groenemeijer, P., Kuhne, T., Radler, A.T., Antonescu, B., Faust, E. Large hail incidence and its economic and societal impacts across Europe. Monthly Weather Review, 2019, 147(11), 3901–3916.

[10] Litta, A.J., Mohanty, U.C., Sumam, I. The diagnosis of severe thunderstorms with high-resolution WRF model. Journal of Earth System Science, 2012, 121, 297–316.

[11] Thakur, S., Mondal, I., Ghosh, P.B., De, T.K. Thunderstorm characteristics over the northeastern tegion (NER) of India during the pre-monsoon season, 2011 using geosynchronous satellite data. *In:* Abraham, A., Dutta, P., Mandal, J., Bhattacharya, A., Dutta, S. (eds) Emerging technologies in data mining and information security. Advances in Intelligent Systems and Computing, 813. Springer, Singapore, 2019.

[12] Basu, G.C., Mondal, D.K. A forecasting aspect of thundersquall over Calcutta and its parameterisation during pre-monsoon season. MAUSAM, 2002, 53(3), 271–280.

[13] Schumacher, R.S., Johnson, R.H. Characteristics of U.S. extreme rain events during 1999–2003. Weather and Forecasting, 2006, 21(1), 69–85.

[14] Park, H.S., Ryzhkov, A.V., Zrni, D.S., Kim, K.E. The hydrometeor classification algorithm for the polarimetric WSR-88D: Description and application to an MCS. Weather and Forecasting, 2009, 24, 730–748.

[15] Okumura, K., Satomura, T., Oki, T., Khantiyanan, W. Diurnal variation of precipitation by moving mesoscale systems: Radar observations in northern Thailand. Geophysical Research Letters, 2003, 30(20), 1–5.

[16] Satomura, T., Yamamoto, K., Sysouphanthavong, B., Phonevilay, S. Diurnal variation of radar echo area in the middle of Indochina. Journal of the Meteorological Society of Japan, 2011, 89A, 299–305.

[17] Chantraket, P., Kirtsaeng, S., Detyothin, C., Nakburee, A., Kasem, M. Characteristics of hailstorm over northern Thailand during summer season. EnvironmentAsia Journal, 2015, 8(1), 101–114.

[18] Mahavik, N., Tantanee, S. Seasonal characteristics of precipitating cloud properties and structure derived from TRMM: 16 years over the inland of the Indochina Peninsula. Geographia Technica, 2021, 16(1), 48–66.

[19] Dolan, B., Rutledge, S.A. A theory-based hydrometeor identification algorithm for X-band polarimetric radars. Journal of Atmospheric and Oceanic Technology, 2009, 26(10), 2071–2088.

[20] Dolan, B., Rutledge, S.A., Lim, S., Chandrasekar, V., Thurai, M. A robust C-band hydrometeor identification algorithm and application to a long-term polarimetric radar dataset. Journal of Applied Meteorology and Climatology, 2013, 52(9), 2162–2186.

[21] Mahavik, N., Tantanee, S. Convective systems observed by ground-based radar during seasonal march of Asian summer monsoon in the middle of Indochina Peninsula. Engineering and Applied Science Research, 2019, 46(4), 318–330.

[22] Jash, D., Resmi, E.A., Unnikrishnan, C.K., Sumesh, R.K., Kumar, S., Sukumar, N. Analysis of pre-monsoon convective systems over a tropical coastal region using C-Band polarimetric radar, satellite and numerical simulation. Atmosphere, 2022, 13(9), 1349.

[23] Doviak, R.J., Zrni, D.S. Doppler radar and weather observations, 2nd Ed, Academic Press: Cambridge, MA, USA, 1993, 562p.

[24] Kumjian, M.R. Principles and applications of dual-polarization weather radar. Part I: Description of the polarimetric radar variables. Journal of Operational Meteorology, 2013, 1(19), 226–242.

[25] Ryzhkov, A., Zhang, P., Bukovcic, P., Zhang, J., Cocks, S. Polarimetric radar quantitative precipitation estimation. Remote Sensing, 2022, 14(7), 1695.

[26] Vivekanandan, J., Zrni, D.S., Ellis, S.M,, Oye, R., Ryzhkov, A.V., Straka, J. Cloud microphysics retrieval using S-band dual-polarization radar measurements. Bulletin of the American Meteorological Society, 1999, 80, 381–388.

[27] Zrnic, D.S., Ryzhkov, A.V. Polarimetry for weather surveillance radars. Bulletin of the American Meteorological Society, 1999, 80, 389–406.

[28] Chen, Y., Liu, X.E., Bi, K., Zhao, D. Hydrometeor classification of winter precipitation in

northern China based on multi-platform radar observation system. Remote Sensing, 2021, 13, 5070.

[29] Kumjian, M.R., Prat, O.P., Reimel, K.J., van Lier-Walqui, M., Morrison, H.C. Dual-polarization radar fingerprints of precipitation physics: A review. Remote Sensing, 2022, 14(15), 3706.

[30] Kumjian, M.R. Principles and applications of dual-polarization weather radar. Part I: Description of the polarimetric radar variables Journal of Operational Meteorology, 2013, 1(19), 226–242.

[31] Hersbach, H., The ERA5 global reanalysis. Quarterly Journal of the Royal Meteorological Society, 2020, 146, 1999–2049.

[32] Copernicus Climate Change Service, ERA5: Fifth generation of ECMWF atmospheric reanalyses of the global climate. Copernicus Climate Change Service Climate Data Store (CDS), 2017, https://cds.climate.copernicus.eu/cdsapp#!/home. [Accessed 2 December 2020].

[33] Romanick, D., Taszarek, M., Brooks, H.E. Convective environments leading to microburst, macroburst and downburst events across the United States. Weather and Climate Extremes, 2022, 37(8), 100474.

[34] Pilguj, N., Taszarek, M., Allen, J.T., Hoogewind, K.A. Are trends in convective parameters over the United States and Europe consistent between reanalyses and observations?. Journal of Climate, 2022, 35(12), 3605–3626.

[35] Helmus, J.J., Collis, S.M. The Python ARM Radar Toolkit (Py-ART), a Library for working with weather radar data in the Python programming language. Journal of Open Research Software, 2016, 4(1), e25.

[36] Heistermann, M., Jacobi, S., Pfaff, T. Technical note: An open source library for processing weather radar data (wradlib). Hydrology and Earth System Sciences, 2013, 17, 863–871.

[37] Giangrande, S.E., McGraw, R., Lei, L. An application of linear programming to polarimetric radar differential phase processing. Journal of Atmospheric and Oceanic Technology, 2013, 30(8), 1716–1729.

[38] Maesaka, T., Iwanami, K., Maki, M. Non-negative K_{DP} Estimation by monotone increasing PHIDP assumption below melting layer. The Seventh European Conference on Radar in Meteorology and Hydrology, 2012.

[39] Gu, J., Ryzhkov, A., Zhang, P., Neilley, P., Knight, M., Wolf, B., Lee, D. Polarimetric attenuation correction in heavy rain at C Band. Journal of Applied Meteorology and Climatology, 2011, 50(1), 39–58.

[40] Tessendorf, S.A., Miller, L.J., Wiens, K.C., Rutledge, S.A. The 29 June 2000 supercell observed during STEPS. Part I: Kinematics and microphysics. Journal of the Atmospheric Sciences, 2005, 62(12), 4127–4150.

[41] Liu, H., Chandrasekar, V. Classification of hydrometeors based on polarimetric rRadar measurements: Development of fuzzy logic and neuro-fuzzy systems, and in situ verification. Journal of Atmospheric and Oceanic Technology, 2000, 17(2), 140–164.

[42] Ryzhkov, A.V., Schuur, T.J., Burgess, D.W., Heinselman, P.L., Giangrande, S.E., Zrnic, D.S., The ioint polarization experiment: Polarimetric rainfall measurements and hydrometeor classification. Bulletin of the American Meteorological Society, 2005, 86, 809–824.

[43] Chandrasekar, V., Keranen, R., Lim, S., Moisseev, D. Recent advances in classification of observations from dual polarization weather radars. Atmospheric Research, 2013, 119, 97–111.

[44] Kiguchi, M., Matsumoto, J. The rainfall phenomena during the pre-monsoon period over the Indochina Peninsula in the GAME-IOP Year, 1998. Journal of the Meteorological Society of Japan, 2005, 83(1),.89–106

[45] Obayashi, F., Kikuchi, K. A Microburst phenomenon in Kita Village, Hokkaido on September 23, 1986. Journal of the Meteorological Society of Japan, 1989, 67(5), 925–936.

[46] Atkins, N.T., Justin, M.A., Przybylinski, R.W., Wolf, R.A., Ketcham, B.D. Vortex structure and evolution within bow echoes. Part I: single-doppler and damage analysis of the 29 June 1998 derecho. Monthly Weather Review, 2004, 132, 2224–2242.

[47] Nowotarski, C.J., Peters, J.M., Mulholland, J.P. Evaluating the effective inflow layer of simulated supercell updrafts. Monthly Weather Review, 2020, 148(8), 3507–3532.

[48] Giangrande, S.E., Ryzhkov, A.V. Estimation of rainfall based on the results of polarimetric echo classification. Journal of Applied Meteorology and Climatology, 2008, 47, 2445–2462.

[49] Duda, J.D., Gallus, W.A.Jr. Spring and summer midwestern severe weather reports in supercells compared to other morphologies. Weather and Forecasting, 2012, 25(1), 190–206.

[50] Parker, M.D., Johnson, R.H. Organizational modes of midlatitude mesoscale convective systems. Monthly Weather Review, 2000, 128(10), 3413–3436.

[51] Zhang, H., Rao, X., Guo, Z., Liu, X., Yu, X., Chen, X., …, Chen, S. Detailed evolution charac-

teristics of an inclined structure hailstorm observed by polarimetric radar over the south China Coast. Atmosphere, 2022, 13(10), 1564.

[52] Straka, J.M., Zrni, D.S., Ryzhkov, A.V. Bulk Hydrometeor classification and quantification using polarimetric radar data: Synthesis of relations. Journal of Applied Meteorology and Climatology, 2000, 39, 1341–1372.

[53] Kumjian, M.R., Khain, A.P., Benmoshe, N., Ilotoviz, E., Ryzhkov, A.V., Phillips, V. The anatomy and physics of ZDR columns: Investigating a polarimetric radar signature with a spectral bin microphysical model. Journal of Applied Meteorology and Climatology, 2014, 53, 1820–1843.

[54] Kuster, C.M., Schuur, T.J., Lindley, T.T., Snyder, J.C. Using Z_{DR} columns in forecaster conceptual models and warning decision-making. Weather and Forecasting, 2020, 35, 2507–2522.

[55] Li, X., Mecikalski, J.R., Otkin, J.A., Henderson, D.S., Srikishen, J. A polarimetric radar operator and application for convective storm simulation. Atmosphere, 2022, 13(5), 645.

[56] Aydin, K., Seliga, T., Balaji, V. Remote sensing of hail with a dual linear polarization radar. Journal of Applied Meteorology and Climatology, 1986, 25, 1475–1484.

[57] Holler, H., Bringi, V., Hubbert, J., Hagen, M., Meischner, P. Life cycle and precipitation formation in a hybrid type hailstorm revealed by polarimetric and doppler radar measurements. Journal of the Atmospheric Sciences, 1994, 51, 2500–2522.

[58] Satomura, T. Diurnal variation of precipitation over the Indo-China Peninsula: Two-dimensional numerical simulation. Journal of the Meteorological Society of Japan, 2000, 78, 461–475.

[59] Carbone, R.E., Tuttle, J.D., Ahijevych, D.A., Trier, S.B. Inferences of predictability associated with warm season precipitation episodes. Journal of the Atmospheric Sciences, 2002, 59, 2033–2056.

[60] Pocakal, D., Vecenaj, Z, Jurkovic, P.M., Grisogono, B. Analysis of orographic influence on hail parameters in NW Croatia. International Journal of Climatology, 2018, 38(3), 5646–5658.

[61] Kunz, M., Fluck, E., Baumstark, S., Wandel, J., Ritz, S., Schemm, S., Schmidberger, M. Hail frequency in central Europe estimated from 2D radar data and the relation to atmospheric characteristics. 9th European Conference on Severe Storms (ECSS), 18–22 Sept. 2017, Pula, Croatia. Wessling, Germany: European Severe Storms Laboratory, 2017.

[62] Lang, T.J. Python-based scientific analysis and visualization of precipitation systems at NASA Marshall Space Flight Center. Fifth Symposium on Advances in Modeling and Analysis Using Python. 5 January 2015, Phoenix, Arizona, USA, 2015, 1–21.

[63] Williams, J.K., Cornman, L.B., Yee, J., Carson, S.G., Blackburn, G., Craig, J. NEXRAD detection of hazardous turbulence. 44th AIAA Aerospace Sciences Meeting and Exhibit, 2006, AIAA 2006-76.

[64] Labitt, M. Coordinated radar and aircraft observations of turbulence, Project Report ATC-l08, Lincoln Laboratory, Massachusetts Institute of Technology, 1981.

[65] Lang, T.J. Single Doppler Retrieval Toolkit (SingleDop), Environmental Science Earth Air Space Exoplanet, 2023. [Online] Available from: https://github.com/nasa/SingleDop

[66] Wheatley, D.M., Trapp, R.J., Atkins, N.T. Radar and damage analysis of severe bow echoes observed during BAMEX. Monthly Weather Review, 2006, 134(3), 791–806.

[67] Wakimoto, R.M., Murphey, H.V., Davis, C.A., Atkins, N.T. High winds generated by bow echoes. Part I: Overview of the Omaha bow echo 5 July 2003 storm during BAMEX. Monthly Weather Review, 2006, 134, 2793–2812.

[68] Mathias, L., Ermert, V., Kelemen, F.D., Ludwig, P., Pinto, J.G. Synoptic analysis and hindcast of an intense bow echo in western Europe: The 9 June 2014 Storm. Weather and Forecasting, 2017, 32(3), 1121–1141.